19th Australasian Fluid Mechanics Conference
Melbourne, Australia
8-11 December 2014

Development of a Drag Reduction System (DRS) For Multi-Element Race Car Wings

S. Wordley, D. McArthur, L. Phersson, D. Tudball Smith and D. Burton.

Department of Mechanical and Aerospace Engineering,
Monash University Clayton, VIC 3800, Australia

Abstract

The design and development of an active Drag Reduction System (DRS) for multi-element wings in a race car application is described. Such systems are currently allowed within certain racing categories, including Formula 1, and provide the opportunity to run increased downforce levels for cornering and braking events, whilst minimising drag during straight line acceleration. Switching from the high downforce to the low drag mode is achieved by individual rotation of the trailing edge flaps. This aerodynamically decouples the multi- element configuration and converts it to a staggered multi-plane assembly, reducing the lift-induced drag produced by the wing. In the present example, DRS is applied to both the front and rear wings of the car in an effort to retain an acceptable aerodynamic balance when the system is deployed, thereby retaining aerodynamic stability and allowing DRS to be used in partial cornering situations. Numerical models are developed to predict the quasi-static aerodynamic performance of the wings in isolation as the flaps are progressively rotated. These results are correlated with full scale wind tunnel tests.

Maximum drag reductions of 70% and 83% are predicted for the front and rear wings respectively. Downforce was found to be reduced by 37% for the front and 67% for the rear wing, with the large difference attributed to the fact that the front wing is operating in ground effect. A numerical simulation of the full car with front and rear wings, driver and underbody diffuser predicted that the application of DRS resulted in a maximum full car drag reduction of 62%. However this mode was found to produce an unacceptably large forward shift in the aero balance, which would make the car extremely unstable and prone to over steer. By reducing the magnitude of DRS applied to the rear wing a configuration was found which slightly improved the aerodynamic balance and stability of the car at high speeds whilst still delivering a total drag reduction of 54%.

Introduction

Inverted airfoils and underbody diffusers are commonly used on race cars to generate negative lift or "downforce" which increases the normal load on the tires, resulting in improved lateral and longitudinal acceleration potential. The use of such devices generally results in increased vehicle weight and aerodynamic drag, both of which act to reduce straight line acceleration and the drag limited top speed of the vehicle. Due to these competing influences and assuming the use of traditional fixed, rigid aerodynamic devices, a unique compromise must be made between the weight, downforce and drag produced by an aerodynamic package in order to achieve optimum performance. However, where allowed, the use of actively controlled aerodynamic devices allows both high downforce and low drag modes to be applied when desired. Such modes may alternate discretely or be fully automated and continuously variable with the use of modern high speed sensors and control systems.

Such ideas are not new to racing. Jim Hall's 1966 Chaparral 2E featured a large single element inverted airfoil with its incidence dynamically controlled by the driver via a pedal, allowing high angle of attack and high downforce for cornering and braking and a low angle of attack and reduced drag for the straights [1]. This solution changed the design paradigm for race cars by demonstrating the vital importance of downforce on race car performance. However due to a number of high profile accidents and the complaints of fellow competitors, actively controlled aerodynamic devices were quickly banned in nearly all forms of motorsport.

In 2011, in a bid to increase the opportunities for passing, Formula 1 re-introduced actively controlled aerodynamics in the form of a Drag Reduction System (DRS) for the rear wing [2]. This system was essentially a moveable flap on the rear wing which could be turned out to reduce drag along the straights. Unlike a typical commercial aircraft wing which uses a multi-element configuration that retracts into a single element configuration, race cars have adopted a different approach. As most race car wings are simply supported between endplates and skin friction is of little consequence, a reduced drag (and downforce) configuration can be achieved more easily by rotating and aerodynamically decoupling each element within an existing multi-element configuration. When each element is rotated to ~0° angle of attack, the assembly becomes multi-plane with both vertical spacing and stagger of the order of the flap chord lengths. The effectiveness of these systems has inspired various road car manufacturers and after- market suppliers to re-examine and develop actively controlled wings. There is also growing interest in actively controlled aero amongst Formula SAE and Formula Student competitions, which have always allowed such devices [3]. In 2011 at the FSAE-WEST competition the Oklahoma Formula SAE team (Sooner Racing) debuted the first actively controlled wings seen in Formula SAE history, with front and rear wing flaps dynamically actuated by micro-servos [4].

The current authors have published extensively on the design, development and validation of aerodynamic devices for the Formula SAE competition [5,6,7]. This work draws heavily upon the research and techniques outlined by McBeath [8] and Katz [9]. The 2011 rules for this competition [3] allow for substantial front and rear wings, underbody diffusers, unsprung mounting of aero components (direct to the outboard suspension to minimize ride stiffness increases) and active control of any aerodynamic devices. Powered Ground Effects, such as "sucker" fans, are however prohibited.

Wing Specifications

The front and rear wings of the 2011 Monash Formula SAE car were used in this study. These wings are multi- element designs, with each comprising a large mainplane and dual trailing edge flaps. The front wing operates in ground effect and is partially

divided by the nose cone, with only the mainplane completing the full wing span. Substantial endplates are used on both wings and these are fitted with side gurneys and footplates on the outboard sides. Inner endplates are used to support the inboard side of the front flaps close to the nose cone. Both wings are mounted unsprung in order to maintain a consistent ground clearance with vehicle pitch and ride motions and also to deliver the aero loads directly to the wheels. The wing profiles were developed based on detail modification of the family of profiles proposed by Enrico Benzing [10]. Flap angles, slot gap clearances and overlaps were determined via a parametric CFD study. A summary of the final wing specifications are provided in the table below.

Specification	Front Wing	Rear Wing
Number of Elements	3 ends, 1 centre	3
Aspect Ratio	2.67	1.33
Flap Lengths (Ch)	26%	20%
Gurney Heights (Ch)	3%	2%
Design AoA (°)	26°	24°

Table 1. Wing specifications.

Numerical Formulation

Steady-state RANS simulations were performed using the commercial code ANSYS, with CFX used as a flow solver. For the front and rear wings analysed in isolation, the computational domain was set ~5 chord lengths in front of, ~8 chord lengths above and ~10 chord lengths behind the wing models. A total domain width of ~10 chord lengths was used. The rear wing profiles were located 1.0 chord length above the moving ground, and the front wing profiles 0.1 chord length above the moving ground. The inlet condition was set to a constant velocity of 16.7 m/s (based on an average track speed of 60 km/h) with 1 % turbulence intensity. This results in a Reynolds number of approximately 10^7 for the rear wing in isolation. A half domain with a symmetry plane condition was used. The boundaries representing the wing models were modeled as no slip and the remaining domain walls were set as free slip.

Full car CFD simulations were performed in a similar manner, with a moving ground boundary condition and a domain size of the same relative proportions based on vehicle length. The full car geometry was simplified in order to bring the required computational resources down to a reasonable level. Radiators were not modeled and the exposed engine and intake system was simplified.

The domain close to the models was meshed using a heavily refined unstructured tetrahedral mesh to simplify meshing the complicated geometries, with a 7 layer prismatic inflation layer to capture the boundary layer forming over the surfaces of the car and wings. Hexahedral elements were used in the angled wake refinement region to capture and resolve vortex structures in the large up-wash. A coarse unstructured tetrahedral mesh was used in the far field. A mesh resolution study produced a refinement which resulted in mesh counts of ~12 million elements for the wing in isolation symmetry models and ~35 million elements for the full car symmetry model. y+ values reached localised maxima of around 40 in high velocity regions but averaged less than 20 over most of the geometry.

A Shear Stress Transport turbulence model was used and convergence monitored through momentum and mass residuals as well as force measurements. Simulations were run well beyond the convergence limits to ensure solution stability.

Wind Tunnel Testing

A range of measurements were conducted to validate the performance of the rear wing in isolation with and without DRS using the Monash University Full Scale Wind Tunnel. The facility is a closed return, ¾ open jet wind tunnel with a working section nozzle of 2.6m height and 4.0m width. Full flow properties and specifications for this wind tunnel are described by Gilhome [11]. The front wing was not wind tunnel tested in isolation due to the lack of moving ground simulation.

The rear wing was first set at its design angle of attack (24°) with the flaps in the standard position. Both flaps were then progressively "turned out" until horizontal. In a separate series of tests only the rear most flap was rotated on its own, with the middle flap closest to the mainplane remaining in its design position. Dynamic actuation and response tests were also conducted, videos of which are accessible online [12].

Results and Discussion

Drag polars comparing CFD and experimental (wind tunnel) results for full the range of DRS positions for the rear wing in isolation are provided in figure 1.

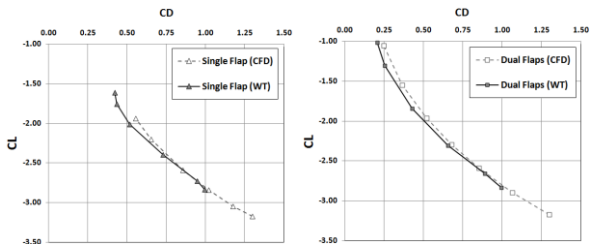

Figure 1. Rear wing drag polars. Wind tunnel vs. CFD correlations for single flap (left) and dual flap (right) rotation.

Figure 2 shows the effect of actuating the DRS on the velocity field at the centre plane of the wing. With the flaps unrotated (figure 2a) there is, as expected, a large velocity differential between the top and bottom surfaces of the wing and a clearly visible upwash as seen throughout the vector field in the wake. Actuating the DRS to the 50% position shows a clear reduction in this velocity differential, with velocities closer to the freestream value (V/V_∞ closer to 1) and a clear reduction in upwash, resulting in respective lift and drag reductions to 72.6% and 52.3% of their original values (figure 3). This shows a drag reduction that is the square of the lift reduction, a result that confirms a significant reduction in lift-induced drag which is expected to vary with lift squared.

The minimal drag position in figure 2c shows a further reduction in velocity differential across the wing's flow field, with a heavy reduction in upwash resulting in lift and drag reductions to 33.4% and 16.9% of their original values (figure 3). This result is slightly less than a squared relationship between lift and drag as seen in the 50% actuated position, however it is observed in this configuration there is a leading edge separation bubble over the top surface of the middle and top flaps. Despite this separation region, this is the maximum drag reducing position due to further reductions in induced drag, however overall reductions may be limited by the separation region and any other profile drag produced by the system. Further rotation of the flaps (figure 2d) shows an increased separation region with only a minor reduction in lift (6.6% lift reduction compared to 100% actuation), as such an increase in drag can be seen as it is no longer possible to reduce lift-induced drag through flap rotation without incurring a larger increase in separation drag.

The result of single flap actuation is similar, with lift and drag reductions to 85.6% and 72.3% of their original values when the flap actuation is 50% (figure 2f), again exhibiting a squared relationship. While at its highest drag reduction rotation, figure 2g, lift and drag reductions are to 61.2% and 42.3% of their

original values, falling below the lift-squared reduction expected by purely lift-induced drag, again most likely caused by the leading edge separation encountered from the slightly negative relative angle of incidence of the rotated top flap in the upwash of the mainplane and middle flaps.

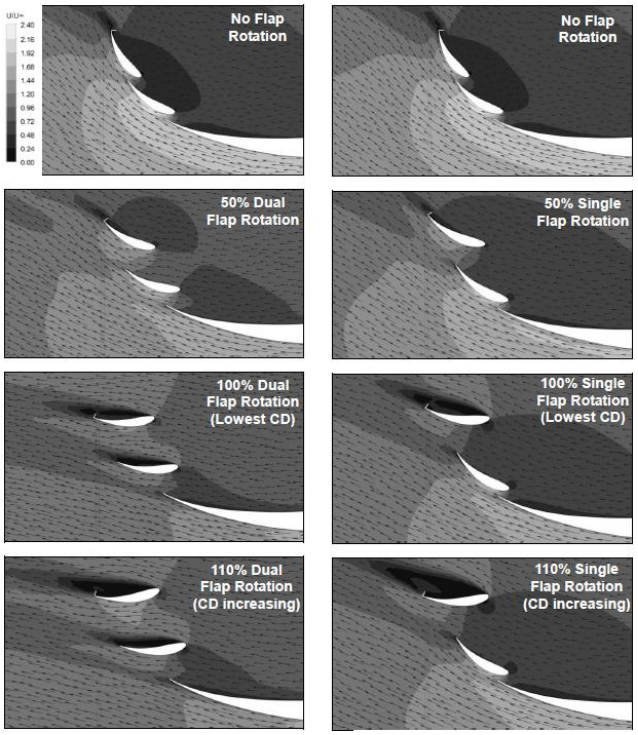

Figure 2. Rear wing symmetry plane velocity field, Dual flap rotation(left) and Single flap rotation(right).

The comparison between single and dual flap rotation is shown in figure 1, where the drag polars produced by both CFD and wind tunnel are compared. This shows that at lower DRS settings (bottom right of the drag polar curve) the lift- drag characteristics of the wing are similar for single or dual flap rotation, with a slight deviation into lower efficiency for the fully actuated single flap (likely caused by the separation bubble or flow disturbance off the middle flap trailing edge). The dual flap, however, produces an overall larger maximum drag (and corresponding lift) reduction when fully actuated. From this it is seen that if only mild drag reductions are required, it may be equally well achieved with a single flap rotation, simplifying the required actuation system, while high drag reductions are only achieved when actuating both flaps with the added penalty of further reduced downforce.

Figures 3 and 4 also show the relative reduction of drag and downforce for each of the four components of each wing: flaps, mainplane and endplates. Figure 5a shows that in its standard configuration, 69.2% of the total drag is produced by the middle and top flaps (flap 1 and flap 2 respectively) and that by rotating the flaps throughout the DRS range of actuation, this contribution is reduced to 31.8% of the total drag of this configuration. The contribution of lift from the flaps is 26.2% in the standard configuration and near-zero when fully rotated in the DRS arrangement. This has been explained from a lift-induced drag perspective, but can also be considered from a pressure field and geometric perspective. When the flaps are rotated their aerodynamic influence on the system is reduced, decreasing the pressure differential in the upper region of the wing where the flaps are located. In the standard non-rotated configuration, the flap surfaces (particularly flap 2, the upper flap) are closer to vertical, so that this pressure differential produces mostly drag.

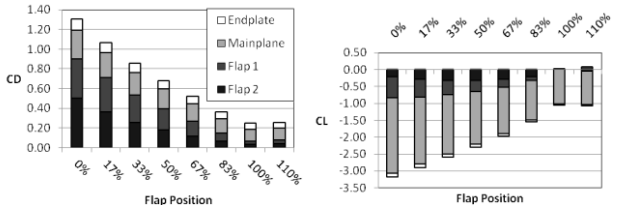

Figure 3. Rear wing component contributions to C_D(left) and C_L(right) as a function of flap rotation angle. Dual flap rotation.

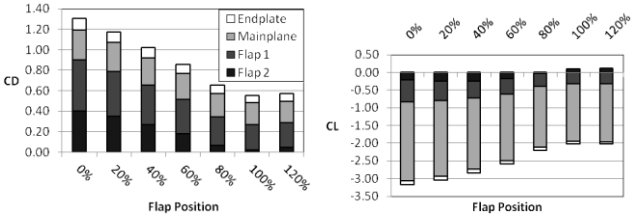

Figure 4. Rear wing component contributions to C_D(left) and C_L(right) as a function of flap rotation angle. Single flap rotation.

Figure 3b also shows an interesting trend, with no actuation, the downforce contribution of the middle flap is high given its small chord compared to the mainplane and during flap rotation. The largest pressure and velocity differential across the wing in the unrotated configuration actually occurs above and below the middle flap. Below the flap, air flowing through the slot gap and off the trailing edge of the mainplane produces this high velocity as seen in figure 3a. Also, the downforce magnitude produced by the upper flap initially increases up to 50% actuation, remains high up to 83% rotation, then drops to near-zero lift production at 100% rotation. This feature can be observed on the velocity fields in figure 2a-c, in the unrotated configuration, there is a pressure difference across the flap, however since it is near vertical, this results mostly in drag. The function of the top flap is to "pump" the air across the middle flap and more vertically, producing a favourable pressure distribution on the middle flap and mainplane, so that even though the lift contribution on a force basis as shown in figure 3b is low, its affect on the flow field as shown throughout figure 2 is large. As the upper flap is rotated, the velocity differential from the top to bottom of the flap is mostly retained, and since the flap is horizontal, its contribution to overall downforce is slightly increased, though its contribution to drag and also the flow field as seen in figure 4 is reduced.

Figure 1 also shows a comparison between wind tunnel and CFD results. The results match closely, falling along a near identical drag polar for much of the range of DRS actuation. The main difference between the wind tunnel and numerical results is that the wind tunnel results do not obtain as high a maximum lift value, and for the single flap case it reduces to a lower lift and drag value for the same flap rotation. There are various differences between the wind tunnel and CFD set up which are unavoidable, such as vibration and freestream velocity profile differences, however it is thought that this difference comes primarily from the limited size of the test section available in the wind tunnel. The wind tunnel is closed return, but with an open test section and nozzle height of only 2.6m. The wing sits in this test section with the bottom surface at 0.9m high and the top of the wing at 1.5m high, and produces a significant upwash and large vortex structures as seen in figure 5c. Such characteristics were observed using smoke visualisation during wind tunnel testing. It is felt that these large structures and upwash are pushing beyond the shear layer produced by the wind tunnel nozzle, pushing the flow upwards into the stagnant air above the test section, and reducing the magnitude of the force coefficients returned experimentally. This theory is further supported by the fact the wind tunnel and CFD results match closely when both

flaps are fully opened (the lowest points in figure 2b), a situation when the upwash and vortex structures are heavily reduced.

CFD results (only) for changing the angle of the front wing flaps were calculated. As with the rear wing, we see a similar proportion of drag reduction as the flaps are rotated into their "full DRS" positions. However, it is observed that the downforce reduction for the front wing in isolation is not as large as that observed for the rear wing. The front mainplane continues to produce large amounts of downforce even when a single flap or both flaps have been fully turned out. This is due in part to the front wing working heavily in ground effect and also because the flaps on the front wing aren't as significant to the overall operation of the wing, given that the flaps do not run full span.

The large difference in front and rear wing downforce reduction due to the application DRS was identified as a major concern, as it could result in a significant forward shift in the aerodynamic balance of the vehicle, causing the vehicle to tend towards increased oversteer. This would reduce vehicle stability and driver confidence, and potentially erode any gains generated by the reduced drag. Additionally, flow structure interaction between the wings, the car and underbody diffusers can also cause further shifts in the aerodynamic balance of the car.

The only way to accurately quantify the effects of all these interactions and determine the final aerodynamic performance and balance is to numerically model or experimentally test the full car with the wings in their final mounted locations. Due to the lack of moving ground simulation in the Monash Wind Tunnel a small number of full car CFD simulations were conducted in an attempt to quantify the aero performance of the entire vehicle and fine tune the proposed DRS. Four different configurations were tested: neutral aerodynamic balance occurs when downforce is split equally between the front and rear tyres. Configurations with greater front downforce represent likely aerodynamic induced "oversteer", and configurations with greater rear downforce indicate likely "understeer" and increased vehicle stability. In most circumstances, it is desirable to slightly increase understeer at higher speeds, to allow the driver to find the grip limit without adverse repercussions (such as a spin).

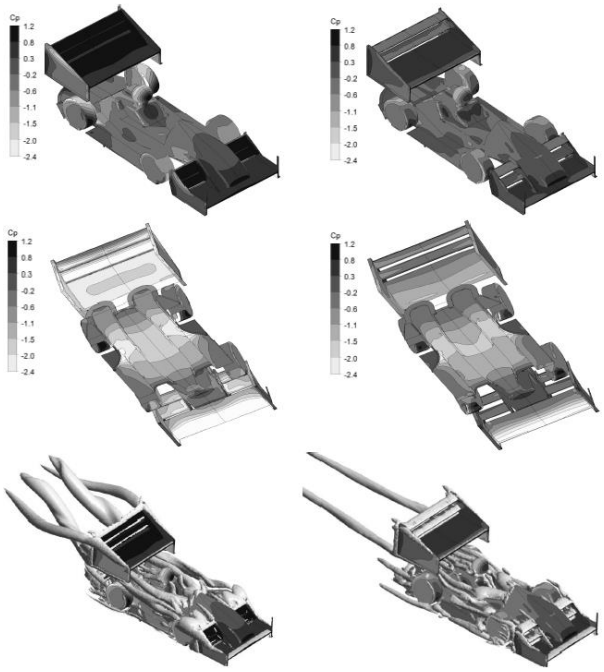

Figure 5. Full car Pressure contours and vortex cores, flaps closed(left) and flaps open(right).

The Full DRS actuation, however, pushes the aerodynamic balance forward by a significant margin (+7% front), which in the authors' experience would decrease stability to an unacceptable level. An intermediate configuration, where both rear wing flaps are rotated to 50% of their full range, results in a much better compromise. This setting sheds slightly less drag than the full DRS mode but maintains much more rear downforce, which results in a slight rearward shift in aero balance and slightly increased high speed stability. Further on-track testing will be required to validate these theories.

Conclusions

A drag reduction system (DRS) for multi-element race car wings was described. Numerical predictions and wind tunnel experiments were in close agreement. A maximum drag reduction of 83% was predicted for a multi-element rear wing operating in free-stream. A different split, multi-element front wing, operating in ground effect and free-stream conditions returned a maximum drag reduction of 70%. When both wings were mounted to an open-wheel racecar, numerical methods predicted a 54% reduction in full car drag due to the application of the DRS. An acceptable ratio of front downforce distribution was able to be maintained for this configuration.

References

[1] Friedman, D., Chaparral: Can-Am & Prototype Race Cars, MotorBooks International, 2005.

[2] FIA, 2011 Formula 1 Regulations, Fédération Internationale de l'Automobile, 2011.

[3] SAE, 2011 Formula SAE Rules, Society of Automotive Engineers, USA, 2011.

[4] Sooner Racing, Sooner Racing Team Gives You Wings! (That Move), uploaded 5/6/11, www.youtube.com/watch?v=7wozSqFXitY

[5] Wordley, S.J., and Saunders, J.W., Aerodynamics for Formula SAE: Initial Design and Performance Prediction, SAE Paper 2006-01-0806.

[6] Wordley, S.J., and Saunders, J.W., Aerodynamics for Formula SAE: A CFD, Wind Tunnel and On- Track Study, SAE Paper 2006-01-0808.

[7] Wordley, S.J., Saunders, J.W. and J. Pettigrew, Aerodynamics for Formula SAE: On-track Performance Evaluation, SAE Paper 2007-01-0897.

[8] McBeath, S., Competition Car Downforce, Haynes Publishers, Somerset, 1998.

[9] Katz, J., Race Car Aerodynamics, Bentley Publishers, USA, 1995.

[10] Enrico Benzing Profili, 3/1/12. www.benzing.it/enrico.profili.htm

[11] Gilhome, B.R., Unsteady and time-averaged near-wake flow over the rear of sedan automobiles, PhD Thesis, Monash University, 2002.

[12] Monash Motorsport, Wind tunnel tests of DRS on a Formula SAE car, uploaded and accessed 6/8/2011. www.youtube.com/watch?v=_wKYK9WUHMk